CHALMERS
UNIVERSITY OF TECHNOLOGY

Thermal Analysis and Battery Modeling of Structural Battery Composites

Master thesis in Electrical Engineering

MENGYU DONG

Department of Industrial and Materials Science
CHALMERS UNIVERSITY OF TECHNOLOGY
Gothenburg, Sweden 2020

Master Thesis 2020

Thermal Analysis and Battery Modeling of Structural Battery Composites

MENGYU DONG

CHALMERS
UNIVERSITY OF TECHNOLOGY

Department of Industrial and Materials Science
Electrical power engineering
Chalmers University of Technology
Gothenburg, Sweden 2020

Thermal Analysis and Battery Modeling of Structural Battery Composites

MENGYU DONG

Supervisors: David Carlstedt, Department of Industrial and Materials Science
Zeyang Geng, Department of Electrical Engineering

Examiner: Prof. Leif Asp, Department of Industrial and Materials Science

Master's Thesis 2020
Department of Industrial and Materials Science
Division of Material and Computational Mechanics
Chalmers University of Technology
SE-412 96 Gothenburg
Telephone +46 31 772 1000

Typeset in LaTeX
Printed by Chalmers Reproservice
Gothenburg, Sweden 2020

Thermal Analysis and Battery Modeling of Structural Battery Composites
Mengyu Dong
Department of Industrial and Materials Science
Chalmers University of Technology

Abstract

A thermo-electrochemical finite element analysis (FEA) of a structural battery is presented. A simplified model was developed based on a one-dimensional coordinate in through-thickness direction of the battery. This model simulates the thermal behavior of a structural cell during the (dis)charge cycle. The mathematical model solves the conservation of energy considering heat generations due to only resistive heating. The voltage profile and the heat generation of a structural battery cell with active materials: Carbon fiber/LiFePO4 were studied at different discharge rates. The temperature profile from the pseudo two dimensional (P2D) thermo-electrochemical model had a similar tendency to that from the 3D thermo-mechanical model. The temperature profile was illustrated at several discharge rates. It was found that the contribution of heat source due to resistive heating was extensive at a high discharge rate. Also the thermal impact of convection condition on the structural battery was analyzed.

Keywords: Structural battery, Thermal behavior, Heat generation, Heat exchange, Natural convection

Acknowledgements

Many people have contributed to the development of this project and it is a pleasure to acknowledge my indebtedness to a few of them.

First and foremost, I would like to thank my supervisors David Carlstedt and Zeyang Geng for their support and guidance throughout all the ups and downs in the thesis work. I would also like to thank Leif Asp, Johanna Xu, Shanghong Duan, and my co-workers in structural battery group for continually discussions and feedback during our meetings. Lastly, and most importantly I would like to thank my partner Natasha Svensson for standing beside me to study battery thermal performance together.

Nomenclature

A_{cell}	Cross-section area of the P2D-model	m^2
c_s	Li concentration in active materials of electrodes	mol/m^3
$c_{Li,max}$	Maximum Li-concentration	mol/m^3
$c_{Li,ini}$	Initial lithium ions concentration	mol/m^3
$c_{Li,ref}$	Reference lithium ions concentration	mol/m^3
C_p	Specific heat capacity	J/kgK
D_{Li}	Diffusion coefficient of Li^+	m^2/s
D_e	Diffusion coefficient of the structural battery electrolyte (SBE)	m^2/s
t_+	Lithium ions transport number in electrolyte	$-$
V_{epss}	Solid phase (fibers or particles) volume fraction	$-$
V_{epsl}	Solution phase (electrolyte/SBE) volume fraction	$-$
j_0	Exchange current density	A/m^2
j_{loc}	Local current density	A/m^2
h	Heat transfer coefficient	W/m^2K
k	Thermal conductivity	W/mK
η	Overpotential of surface due to charge transfer	V
S_a	Specific surface area	m^{-1}
F	Faraday constant	C/mol
R	Gas constant	$J/Kmol$
T	Absolute temperature	K
b	Constant value for the specific surface area of material particles	$-$
v	Volume	m^3
r^f	Radius of carbon fiber	μm
r^p	Radius of LFP particle	μm
Q	Heat generation	J/m^3
n	Number of transferred electrons per mole reactant	$-$
L	Thickness	μm
I	Cell current density related to A_{cell}	A/m^2
t	Time	s
U	Open circuit voltage of electrodes	V
V	Cell potential	V
ΔH	Enthalpy change	J
Greek letters		
α_a	Anodic transfer coefficient	-
α_c	Cathodic transfer coefficient	-
β	Bruggeman coefficient for tortuosity	-

ρ	Density	kg/m^3
σ	Electrical conductivity of solid phase in electrodes	S/m
κ	Ionic conductivity of the electrolyte	S/m
ϕ	Electric potential	V

Subscripts, superscripts and acronyms

0	Initial state
s	Solid phase
e	Solution phase
eff	Effective value
d	Battery domains (electrodes and separator)
i	Transporting constituent (electrolyte and fibers/particles)
m, n	Chemical reaction species
amb	Ambient (temperature)
irr	Irreversible (heat)
r	Reversible (heat)
sur	Surface (temperature)
α	Constant value for particle radius
CCCV	Constant current constant voltage
CF	Carbon fiber
CFRP	Carbon fiber reinforced polymer
FE	Finite element
LIB	Lithium ion battery
NE	Negative electrode
OCV	Open circuit voltage
P2D	Pseudo two dimensional
PE	Positive electrode
SBE	Structural battery electrolyte
SOC	State of charge

Contents

1

Introduction

1.1 Background

Compared to the conventional LIB (lithium-ion battery), the structural battery can not only store energy but also perform well in carrying mechanical loads, which is achieved by combining the properties of LIB technology and laminated carbon fibers composite materials. The composite laminate is formed by incorporating carbon fibers into a polymer matrix material so as to enhance its mechanical performance. Due to the inherent multi-functional capabilities, it has distinct advantages in saving weight of devices on a system-level [1, 2], and have a bright prospect in the development of electric vehicles.

Temperature is one of the most critical factors in operating of battery systems, and should be controlled within a limited range defined by the chemical properties of the materials. At high or low temperature, the cell performance can be substantially affected, and cause side reactions that may limit the battery life, or even worse, break down the battery. Hence, analyzing the thermal behavior to predict its impact on the multi-physics behavior of this structural battery composite material is crucial and is therefore the key factor of study in this thesis work.

Heat will unavoidably be generated or absorbed in different parts during the charge and discharge cycles of battery systems. During cycling, heat is generated by diverse reactions, such as ohmic losses, kinetic reactions, etc.

1.2 Aim

The aim of this thesis work is to study the thermal behavior of the structural battery during electrochemical cycling, including setting up a battery model in the commercial finite element (FE) software COMSOL to predict the thermal impact on the multi-physics behavior of the structural battery material. The results from the battery model will be compared with the results from a 3D thermo-mechanical model developed in another MSc thesis running in parallel [3].

1.3 Problem statement

This thesis work is conducted around the structural material carbon fiber reinforced polymer (CFRP), and mainly investigated by numerical modeling.

In the first stage, the study pertains to battery modeling. Starting with the electrochemical analysis, a Pseudo-two-dimensional model (P2D) will be developed in COMSOL to model the battery cell chemistry. Compared with the thermo-mechanical model (developed in parallel), the P2D model is used to derive the generated or absorbed heat due to electrochemical processes during electrochemical cycling. It adopts porous electrode theory and concentrated solution theory, and has become a popular method for battery performance investigations.

Secondly, the thermal behavior of the structural battery is investigated, including calculating the heat generated inside the cell during electrochemical cyclings and the heat transferred between the battery surface and surroundings, separately.

1.4 Scope

This thesis covers a complete design of the structural battery. With the P2D model built in COMSOL, it is possible to predict and evaluate the thermal behavior during electrochemical cycling and the influence on its multi-functional performance.

Not only the actual temperature of each cell but also the temperature differences among the cells would result in different performance and aging rates [3]. Due to the limitation of time and cost, battery cooling systems and degradation analysis will not be studied.

2
Theory

The focus of this research is on the thermal behavior of the structural battery during electrochemical cycling and its impact on the electrical and mechanical performance. In this chapter, basic theoretical knowledge including battery chemistry, battery modeling, and thermal analysis are introduced.

2.1 The Electrochemical cell

Normally, multiple cells are connected in series or parallel to operate as a form of battery module/pack in order to enhance voltage/energy capability and to maintain the output power requirements in service. Thus, the electrochemical cell can be seen as the most fundamental unit in a battery.

As shown in Figure 2.1, an electrochemical cell can be called either electrolytic or galvanic. An electrolytic cell is transferring electrical energy to chemical energy (charging of the battery); A galvanic cell is converting chemical energy into electrical energy (discharging of the battery). Based on different capabilities, a cell can be identified as a primary cell (only galvanic) or a secondary cell. The latter is also known as a rechargeable cell, which has both galvanic and electrolytic reactions.

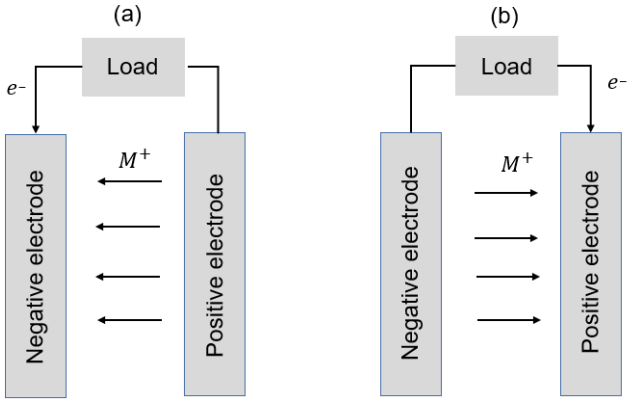

Figure 2.1: (a) An electrolytic cell (b) a galvanic cell (both retrieved from [4])

In redox batteries, energy is transferred via redox reactions that occur at the surface of cells. During discharge, the oxidation reaction takes place at the negative

electrode surface by losing electrons continuously to the positive electrode via an external circuit. The reduction reaction takes place at the surface of the positive electrode by accepting the electrons. At the same time, ions flow in the same direction inside the battery to maintain charge balance. Conventionally, the electrode which offers electrons in discharging can also be named as the anode and the accepting electrons electrode as the cathode. However, the nomenclature of electrodes will change opposite in charge and discharge. To avoid misunderstandings and simplify the terms, only the positive and negative electrodes will be used in this study.

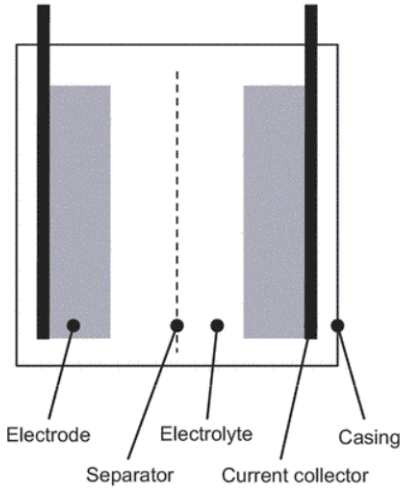

Figure 2.2: The fundamental design of an electrochemical cell from [4]

A cell is composed of several components as schematically illustrated in Figure 2.2. Every component must be designed properly. Poor designs can have a huge negative impact on the cell's overall performance, durability, safety, etc.

2.1.1 Positive electrode

The positive electrode is made of a highly electronic and ionic conductive material, which can be either metallic or insertion types. The metallic electrodes are not very common. Instead, mineral-based electrodes are preferably used for high-capacity Li-ion batteries. These are referred to as insertion electrodes (e.g. porous electrodes) which allow lithium atoms to be stored in the active electrode materials within the porous structure of the electrode. Therefore, the electrochemical reactions can take place at the surface as well as in the bulk of the electrode.

In battery design, the selection of materials applied in positive electrodes is critical, and different host structures and materials applied can highly affect the battery performance, such as the thermal stability and the rate capability, etc. $LiFePO_4$ (LFP) is the most significant compound in olivine structures, which allows Li-ions transport only in one-dimensional channels. This structure may lead to an inherently limited performance caused by low ion mobility, Nevertheless, some properties

(e.g. price advantage and outstanding stability at high temperatures and C-rates) make LFP attractive in LIB market. Considering the price and performance benefits discussed, LFP is selected as the positive electrode in this research.

2.1.2 Negative electrode

Negative electrode materials can mainly be divided into two types, metallic lithium (Li metal) and insertion or conversion materials. Carbon-based insertion types are the most desirable materials due to proven high chemical stability, especially during lithiation and de-lithiation (charge and discharge) cycles and the relatively lower cost [4].

2.1.2.1 Graphite and carbon fiber

Soft carbons, hard carbons, and graphite are three of the most prevalent choices for the negative electrode material. Soft carbons and hard carbons are amorphous, while graphite has a crystalline structure, which is the main difference as well. Their different carbon structure determines the diverse electrochemical performance of a battery, both the capacity and rate capability.

Depending on the production process and raw materials used, carbons can be made of different macroscopic shapes, flakes (graphite), spheres, fibers, etc. Graphite has a crystalline structure of hexagonal carbons packed in graphene layers. When it is fully charged, lithium inserted inside is at an equilibrium state, i.e. LiC_6, where one lithium atom is surrounded by six carbon atoms.

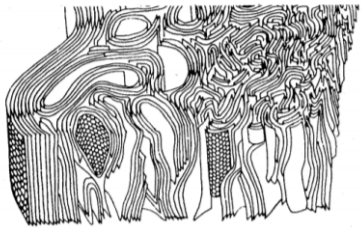

Figure 2.3: Carbon fiber internal structure from [5]

Graphite has been dominating the materials market for Li-ion cells as a result of relatively low cost and simple manufacturing process, but carbon fibers have been found to work as an excellent negative electrode due to the enhanced mechanical performance. For this reason, it is selected as negative material in this research to investigate the impact on the battery's multi-functional performance. Unlike graphite, carbon fibers can be combined with a polymer matrix (CFRP) to create a structural material with superior mechanical integrity. This composite material enjoys distinct advantages in saving the weight of devices on a system-level to maintain the rising need for commercialization. In Figure 2.3, a schematic illustration

of the internal structure of a carbon fiber is presented [5]. Carbon fibers generally exhibit superior tensile and compressive strength, and that's why it can store energy and carry a mechanical load at the same time [6].

2.1.3 Separator and electrolyte

A separator has two main functions, prevent the direct contact of electrodes to avoid internal short circuits, while allowing ion transport within the cells [7]. In conventional batteries, the separator is usually made of a porous polymer film that allows high ion conductivity of the electrolyte to ensure the electrochemical performance inside the battery, and also behaves as an electronic insulator.

As for the structural battery, a newly developed electrolyte has been applied in this case, known as the structural battery electrolyte (SBE) [8, 9]. It consists of two parts, a stiff porous thermoset matrix made of polymer soaked with liquid electrolyte with Li salt. The liquid in this polymer network enables ion transport between the electrodes, while the solid matrix material makes it possible to distribute mechanical loads.

2.1.4 Current collectors

The main function of current collectors is to transfer electrons between electrodes via an external circuit in the battery [10]. To achieve this, an adhesive binder including conductive particles (e.g. carbon black) can be utilized to apply electrode materials onto them. Therefore, to minimize energy losses caused by cell impedance and keep inactive in direct contact with the active materials, current collectors are required to possess high electrical conductivity and electrochemical stability in this process.

There are three types of current collectors that are commercialized, mesh, foam, and foil. Metallic foils are relatively popular among these since they are thin and lightweight, which enables them to provide the increased volumetric capacity of batteries. For the structural battery, each carbon fibers in the negative electrode act as current collectors.

2.2 Battery glossary

Some basic definitions related to the Li-ion battery and its management system are listed in this section.

2.2.1 Voltage hysteresis

It points to the discordance between the charge and discharge behaviors of battery in operation. For example, compared to the charge reactions supported via an

external source, the chemical and electrochemical reactions inside the cell are much slower (e.g. mass transport). Therefore, a voltage difference caused by kinetics and diffusion differences of active species may be observable in charge and discharge cycles. The high current level of the battery would severe this phenomenon and cause a loss of energy and capacity of the battery.

2.2.2 Open circuit voltage (OCV)

It refers to the voltage between positive and negative electrodes when disconnecting these two terminals with any charging device (i.e. no current flow in or out of the battery).

2.2.3 Bruggeman coefficient (β)

Since the Li^+ diffusion and charge conduction within the solution phase is impeded by the electrode particles, the material properties (i.e. diffusion coefficient, electrical conductivity, ionic conductivity) should be sensitive to the electrode microstructures. The Bruggeman coefficient (linked to the degree of porosity and tortuosity) is applied to do the correction of transport parameters in calibrating the 1D model, which can e.g. be seen in [11, 12].

2.2.4 Current rate (C-rate)

It corresponds to the constant current needed to charge/discharge the cell for a given time. 1C represents that the battery can be fully charged in 1 hour with this current, while 2C corresponds to the doubled charge rate, and the battery can be fully charged in 0.5 hours.

2.3 Battery Thermal Modeling

2.3.1 Governing equations

Based on the study by Doyle et al. [13], the governing equations of the one dimensional (also called as pseudo-two-dimensional, P2D) electrochemical model is listed in the following, including equations for the electrochemical kinetics and main processes (e.g. mass and charge transport) occurring during battery electrochemical cycling. Figure 2.4 is obtained from [11] to illustrate the internal structure of a laminated structural battery; The schematic of the P2D model is depicted in Figure 2.5: 1D (x-direction) Lithium-ion cell model coupled with microscopic (r-direction) solid diffusion particles, the detailed explanation seen in Chapter 3.

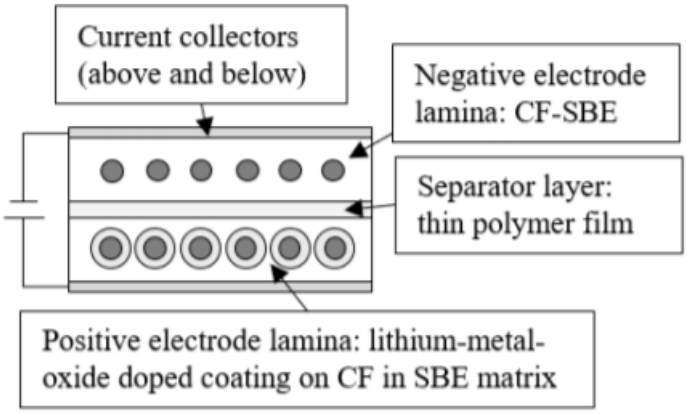

Figure 2.4: Schematic illustration of the laminated structural battery composite architecture, retrieved from [11]

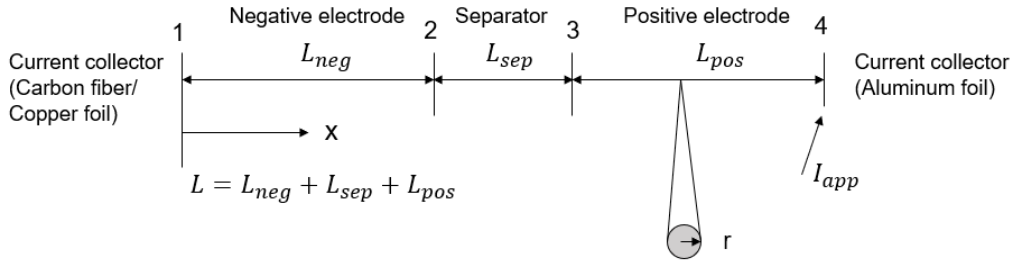

Figure 2.5: Schematic of P2D model: 1D (x-direction) structural cell coupled with microscopic (r-direction) particles

It should be noticed that the dimension (x) defined in Eqs. (2.1),(2.3) and (2.5) is a one-dimensional coordinate system in the through-thickness direction of the battery in Figure 2.5, while the mass transport in the solid phase is defined in the radial dimensional coordinate system (r). This also the reason why this type of model is named as the pseudo-two-dimensional model.

2.3.1.1 Charge balance

Solid phase (in electrodes)

The charge balance in battery electrochemical cycling is defined by Ohm's law, it can be expressed as follows [11, 14]:

$$\frac{\partial}{\partial x}(\sigma_s^{eff}\frac{\partial}{\partial x}\phi_s) = j_{loc}S_a \tag{2.1}$$

$$S_a = \frac{bV_{epss}}{r_s} \tag{2.2}$$

where σ_s^{eff} is the effective electrical conductivity of the solid phase in the electrodes, ϕ_s is the electric potential in the solid phase (fibers of negative electrode,

LFP particles in positive electrode), j_{loc} is the local current density at the electrode surface derived by the Butler-Volmer equation [13]. The specific surface area of material particles is denoted S_a (m^{-1}), where $b = 3$ for herein spherical LFP particles in positive electrode, $b = 2$ for cylindrical CF particles in negative electrode. V_{epss} is the solid phase volume fraction in electrodes, and r_s is the radius of particles.

Solution phase (electrolyte/SBE in electrodes and separator)

The charge balance governing equation is defined as [11, 14]

$$-\frac{\partial}{\partial x}(\kappa_e^{eff}\frac{\partial \phi_e}{\partial x}) + \frac{2RT}{F}(1-t_+)\frac{\partial}{\partial x}(\kappa_e^{eff}\frac{\partial \ln c_e}{\partial x}) = j_{loc}S_a \tag{2.3}$$

where κ_e^{eff} is the effective ionic conductivity of the electrolyte, ϕ_e is the potential of electrolyte, c_e is the lithium salt concentration in the electrolyte, and t_+ is the transport number of lithium ions in the electrolyte.

2.3.1.2 Mass balance

Solid phase
The mass balance of the lithium ions in the particles or fibers is defined by the second Fick's law as [11]

$$\frac{\partial c_s}{\partial t} = \frac{1}{r^\alpha}\frac{\partial}{\partial r}(D_s r^\alpha \frac{\partial c_s}{\partial r}) \tag{2.4}$$

where c_s and D_s is the lithium concentration and diffusion coefficient in the solid phase, respectively. r is the particle radius, $\alpha = 2$ for spherical LFP particles, $\alpha = 1$ in cylindrical fibers.

Solution phase
The mass balance for the solution phase is expressed as

$$\frac{\partial V_{epsl} c_e}{\partial t} = \frac{\partial}{\partial x}(D_e^{eff}\frac{\partial c_e}{\partial x}) + \frac{(1-t_+)}{F} j_{loc} S_a \tag{2.5}$$

where V_{epsl} the volume fraction of solution phase (i.e. electrolyte/SBE) in the electrode and separator, c_e is the lithium salt concentration, D_e^{eff} and t_+ is the effective diffusion coefficient and transport number of lithium ions in the electrolyte.

2.3.2 Boundary conditions

2.3.2.1 Charge balance

Equation (2.1) shows the governing equation of charge balance in solid phase, while Eqs. (2.6 - 2.8) define the charge conditions at each boundary in Figure 2.5.

$$\phi_s|_{x=0} = 0 \tag{2.6}$$

$$\sigma_{pos}^{eff}\frac{\partial\phi_s}{\partial x}|_{x=L} = I_{app} \tag{2.7}$$

$$\sigma_{neg}^{eff}\frac{\partial\phi_s}{\partial x}|_{x=L_{neg}} = \sigma_{sep}^{eff}\frac{\partial\phi_s}{\partial x}|_{x=L_{neg}+L_{sep}} = 0 \tag{2.8}$$

where ϕ_s is set to zero as the electric ground at boundary 1; the charge flux at boundary 4 is assumed to be equal to the average applied current density; Electron flux at boundary 2 and 3 are both zero due to the electronic insulation of separator.

The charge balance in the electrolyte can be expressed as Eq. (2.3), boundary 1 and 4 are external boundaries which are considered to be the insulation point (no flux), while ϕ_e is expected to be continuous at inner boundaries

$$\frac{\partial\phi_e}{\partial x}|_{x=0} = \frac{\partial\phi_e}{\partial x}|_{x=L} = 0 \tag{2.9}$$

2.3.2.2 Mass balance

The mass transport for the lithium ions in the solid particle or fiber phase in the electrodes are governed by Eq. (2.4). Different to other equations defined in a one dimensional coordinate system (x), herein, the lithium ions diffuse in the r-direction. The lithium concentration flux at the center of particles set to zero

$$\frac{\partial c_s}{\partial r}|_{r=0} = 0 \tag{2.10}$$

while, c_s at the particle surface is related to the concentration and flux in the processes occurring in the P2D model (charge and mass transport) in the electrolyte.

Equation (2.5) is the governing equation and defines the material balance in the electrolyte. The external boundaries (1 and 4) are set to have no flux of solution species, and the flux and concentration of solution species are assumed to be continuous at inner boundaries (2 and 3).

2.3.3 Electrochemical kinetics

The charge-transfer process is only occurring at the particle surface, where the local current density of the electrode j_{loc} is one of the critical parameters to characterize, i.e. the charge-transfer reaction between the electrolyte and the active electrode materials. Based on the Butler-Volmer equation, it can be expressed as [11, 13]

$$j_{loc} = j_0(exp(\frac{\alpha_a nF}{RT}\eta) - exp(-\frac{\alpha_c nF}{RT}\eta)) \tag{2.11}$$

$$\eta = \phi_s - \phi_e - E_{eq} \tag{2.12}$$

where j_0 is the exchange current density, α_a and α_c represent the anodic and cathodic charge transfer coefficients, respectively. n is the number of transferred electrons per

mole reactant, herein, $n = 1$. In Eq. (2.12), the overpotential of surface due to charge transfer is denoted η , which is expressed as the difference between the solid and solution phase potentials minus the equilibrium potential of the electrode E_{eq}.

2.3.4 Effective properties

Based on the work by Bruggeman [11, 12], the transport parameters need to be corrected using the Bruggeman exponent related to the degree of porosity and tortuosity of the system, expressed by

$$D_d^{eff} = D_i V_i^{\beta} \tag{2.13}$$

$$\sigma_d^{eff} = \sigma_i V_i^{\beta} \tag{2.14}$$

$$\kappa_d^{eff} = \kappa_i V_i^{\beta} \tag{2.15}$$

2.4 Thermal analysis

The thermal analysis is performed to investigate the generated heat from electrochemical cycling (which is calculated from the electrochemical analysis) and the heat exchange with the surroundings (which is given by the thermo-mechanical model). According to this, the internal heat increased inside a cell can be obtained from the energy balance equation (2.16).

$$Q_{gen} - Q_{diss} = \rho C_p \frac{dT}{dt} \tag{2.16}$$

where ρ is the density, C_p is the specific heat capacity, T is the temperature, t is the time.

2.4.1 Heat source

The heat source inside a cell as derived by Thomas and Newman [15] can be written as

$$Q_{gen} = I(U - V) - IT\frac{dU}{dt} - \sum\nolimits_m \Delta H_m^{avg} R_m - \int \sum\nolimits_n (H_n - H_n^{avg}) \frac{\partial c_n}{\partial t}\, dv \tag{2.17}$$

where I is the current flow in the battery (which is positive on discharging, negative on charging), V is cell voltage, U is the open circuit voltage, ΔH_m and R_m point to the enthalpy change and the rate of chemical reaction m, H_n is the enthalpy of species n, c_n is the concentration of specie n, and v is the volume. The first term refers to the irreversible heat accumulated due to the resistance of all components in the cell when current flows inside the battery, therefore, it can be written as I^2R [16, 17, 18]. The second term is the reversible heat generated by the entropy change of chemical reactions, it could be either positive or negative depending on the direction of current flow and entropy change. Herein, it is more likely observable

at the electrodes where the chemical reactions proceed. The latter two represent the heat generated due to side reactions occurring due to aging, and the heat of mixing due to the concentration gradient within electrodes. Equation (2.17) can be simplified into Eq. (2.18) by making assumptions that the side reactions generating the aging process are very slow and the concentration gradient within the electrodes is negligible [19].

$$Q_{gen} = Q_{irr} + Q_r = I^2R - IT\frac{dU}{dt} \tag{2.18}$$

2.4.2 Heat dissipation

The heat generated inside a cell mainly dissipates in two ways, via conduction and convection. Thermal conduction refers to a direct transfer of heat energy between two objects that are in contact, while heat convection is to dissipate heat by the movement of fluid [20]. Herein, heat conduction is considered to take place inside the battery, and convection is to transfer heat between the battery surface and the surroundings, respectively.

The heat conducting equation is defined by Fourier's law as

$$Q_{cond} = -k\frac{dT}{dx} \tag{2.19}$$

where k is the thermal conductivity of active material, $\frac{dT}{dx}$ is the temperature gradient in x-direction. The negative sign indicates that the heat flow is in the direction of negative temperature gradient.
Equation (2.20) reveals the heat transfer between the surface of the battery and the ambient temperature

$$Q_{conv} = h(T_{sur} - T_{amb}) \tag{2.20}$$

where h is the convective heat transfer coefficient.

3
Case Set Up

3.1 Model development

3.1.1 Model assumptions

For simplicity, the activity dependence and temperature/concentration-dependent terms in material properties are neglected in all battery components. Moreover, the reversible heat is assumed to be zero (canceled term $\frac{dU}{dt}$ in Eq.(2.18)). Besides, the effects of current collectors on electron transport and heat transfer are ignored in this study.

3.1.2 P2D electrochemical model

The P2D electrochemical model in this study is developed based on the model built by Newman, Doyle et al. [13, 21] . According to the porous electrode theory and concentrated solution theory [22], the composite electrodes consist of active materials (solid phase) and electrolyte (solution phase), where the solid phase are the cylindrical (carbon) fibers or spherical particles (LFP), respectively.

The structural battery cell consists of three domains, i.e., a negative electrode (carbon fibers), a polymer electrolyte separator, and a positive electrode (LFP particles and conductive additives), where the electrolyte/SBE is considered extending over the three domains. Figure 2.5 shows the schematic of the P2D model: 1D (x-direction) Lithium-ion cell model coupled with microscopic (r-direction) solid diffusion particles.

3.1.3 Model calibration

3.1.3.1 Model parameters

Table 3.1 lists the model parameters used in the P2D model, including the design specifications, initial and maximum lithium ions concentrations stored in the electrodes, etc.

The diffusion coefficient of lithium ions in the polymer electrolyte, D_e, is calculated from [23],

$$D_e = \frac{2D_{Li^+}D_{PF6^-}}{D_{Li^+} + D_{PF6^-}} = \frac{2 \times 2.5 \times 10^{-13} \times 3 \times 10^{-13}}{2.5 \times 10^{-13} + 3 \times 10^{-13}} = 2.73 \times 10^{-13}(m^2/s) \quad (3.1)$$

Table 3.1: Model parameters for the structural battery

	NE	Separator	PE
Design specifications			
$A_{cell}(m^2)$		1	
V_{epss}	0.4	-	0.48
V_{epsl}	0.6	0.37	0.35
$L(\mu m)$	50	25	55
$r(\mu m)$	2.5	-	1.7
Lithium ion concentrations			
$c_{Li,ini}(mol/m^3)$		1000^a	
$c_{Li,max}(mol/m^3)$	25678^c		21190
$c_{Li,ref}(mol/m^3)$		1	
SOC_{ini}	0.9^b		0.001^b
Kinetic and transport properties			
α	0.5		0.5
β	1.5		2.98
$D_e(m^2/s)$		$(2.73 \times 10^{-13})^d$	
$D_{Li}(m^2/s)$	$(6.8 \times 10^{-13})^c$		3.2×10^{-13}
$\sigma_s(S/m)$	$(6.9 \times 10^4)^c$		91
$\kappa(S/m)$		$(2 \times 10^{-2})^a$	
t_+		0.293	
$F(C/mol)$		96485	
Thermal properties			
$k(W/mK)^e$	50	1	50
$\rho(kg/m^3)$	1850	1100	3600
$C_p(J/kgK)$	750	2300	1500
$T_{ref}(K)$		293.15	

[a] Ref. [8, 9]
[c] Ref. [24]
[d] Calculated from Eq. (3.1)
[b] Calculated from Eq. (3.2)
[e] Lack of source

3.1.4 Voltage range modification

3.1.4.1 Initial conditions for the electrochemical reactions

Figures below show the equilibrium potential profiles for the negative and positive electrodes as functions of the measured SOC. They are used to define the desired voltage range of the cell by selecting proper initial values for electrodes. The potential curve for the negative electrode (carbon fibers) is retrieved from the study by Kjell et al. [24], the positive electrode (LFP particles) profile applies directly from the COMSOL library.

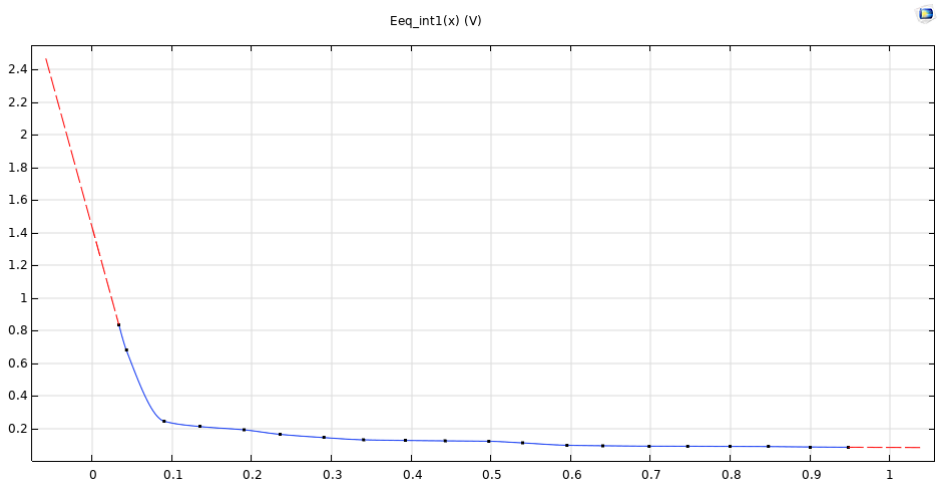

Figure 3.1: Equilibrium potential for CF as function of SOC

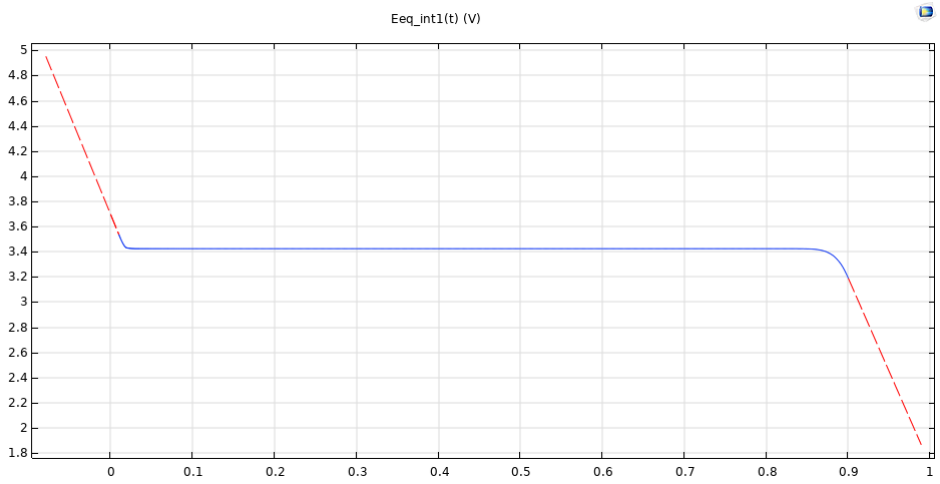

Figure 3.2: Equilibrium potential for LFP as function of SOC

The potential of an electrochemical cell is denoted as the potential difference occurring between the positive and negative electrodes of a cell at the given time. Batteries need to operate in a limited voltage range to protect from overcharging/discharging, it can be normally achieved by setting higher (i.e. 100% SOC) and lower cut-off potentials (i.e. 0% SOC) of the cell separately. Herein, the structural battery cell is initially at a fully charged state, the following equation is applied to define the initial conditions:

$$SOC = \frac{c_{Li,ini}}{c_{Li,max}} \tag{3.2}$$

where the maximum values of lithium concentrations in carbon fibers is based on the study of Kjell, et. al. [24] The initial SOC values for the negative and positive electrodes in the table 3.1 are set as 0.9 and 0.001, respectively, this corresponds to an initial open-circuit voltage of 3.65V (100%SOC of the cell)

Under the initial conditions, a constant current pulse I_{app} is applied at the boundary 4 to discharge the cell, seen in Figure 2.5. The current density of the pulse is set to

12.488 A/m^2, corresponding to 1 C-rate (i.e. the battery can be fully charged in 1 hour with this current) and reads

$$I_{1C} = L_{neg} \times V_{epss.neg} \times \rho_{fiber} \times 0.375[A/g] \times 90\% \tag{3.3}$$

where 0.375 A/g is derived based on the capacity of carbon fiber for 1C current, 90% is the initial coulomb efficiency. It defines as the ratio of the charge extracted from the battery during discharging to the charge transferred during the charging process [25].

3.2 Heat transfer in solids

Assume the structural battery cell is composed of three layers of materials, and the material properties (e.g. the thermal conductivity, heat transfer coefficient, etc.) of each layer are anisotropic. Therefore, the heat dissipation inside the cell should be investigated in different directions. The heat transfer in solids in three-dimensional simulations can be seen in another MSc thesis, conducted by Natasha, who is focusing on the thermo-mechanical modeling of the structural cell [3]. Considering the complexity to do the coupled analysis by combining the 3D thermo-mechanical model (built by Natasha Svensson [3]) and the 1D electrochemical model, herein, the heat generated in the 1D electrochemical model is only considered to be transferred in solids in one dimension (in the through-thickness direction (x) in Figure 2.5), while assuming isotropic material properties for each layer.

3.2.1 Boundary conditions

It is assumed that the structural battery cell is surrounded by air and the convective heat flux is through the external boundaries (boundaries 1 and 4), the initial heat transfer coefficient h is set as 0 W/m^2K (i.e. no heat exchange with the surroundings).

3.2.2 Initial conditions

The initial temperature of the structural cell is the same as the room temperature, $293K$.

4

Result and Discussion

4.1 Model validation

Considering the spread of COVID-19, it became difficult to do the experimental validation of the thermal behaviors of the structural cell. In this study, two methods are instead used to validate the battery performance in the discharge process, i.e., test the thermal model under different current rates and convection conditions to obtain the temperature results. The results are discussed in the sections below.

4.2 Voltage behavior of the structural battery cell

Figure 4.1 illustrates the potential curve of the structural cell at a discharge rate of 1C. Since the initial state of the cell is assumed to be fully charged, the start time point (0 s) and the ending time (3600 s) corresponds to the higher SOC limit (i.e. SOC = 1) and the lower limit (SOC = 0) separately.

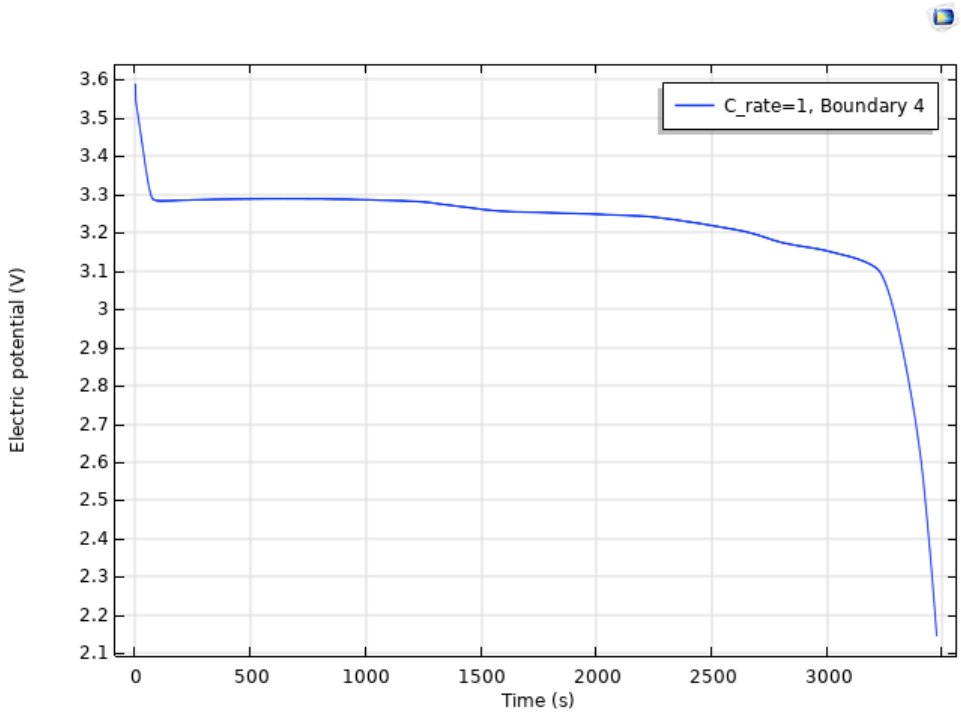

Figure 4.1: Potential curve of the structural battery cell at 1C

To investigate the impact of current magnitude on battery discharge behavior, different current rates are applied to discharge the cell, shown in Figure 4.2.

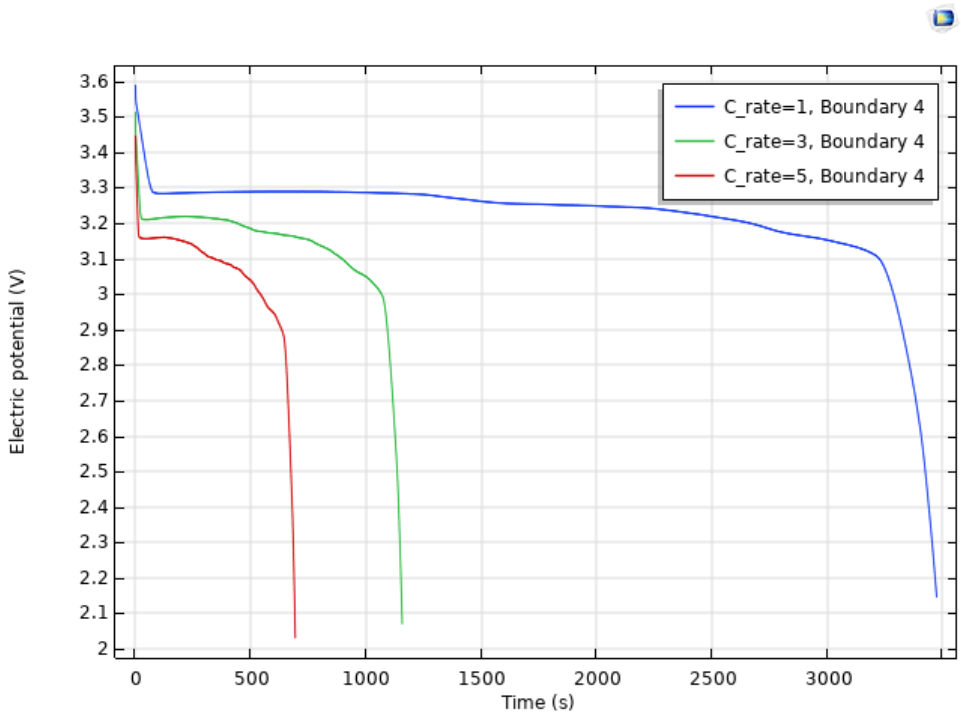

Figure 4.2: Potential curve of the structural cell under different current rates

As the discharge rate increases, the cell potential drops rapidly. Specifically, for low rates, the cell voltage slowly declines and takes 3600 s to drop to the lower limit; For high rates, the potential decreases dramatically, the contours depict the cliff-like drop. This is attributed to the different voltage hysteresis phenomenon, which will be explained below.

The cell voltage in this study can be derived as

$$V_{cell} = U - IR \tag{4.1}$$

where U is the open-circuit voltage of the cell, I is the current flows in the cell, R is the internal resistance of the structural cell. The minus sign points to the voltage losses caused by the cell resistance during discharging. At high rates, the voltage losses caused due to the internal resistance will become substantial, which leads to a shorter time for the cell to drop to the lower limit.

4.3 Thermal behavior of the structural battery cell

4.3.1 Thermal contributions

In order to analyze the thermal behaviors of the structural battery cell at a discharge rate of 1C, the total power dissipated from electrochemical reactions and contributions of heat source are plotted in Figure 4.3.

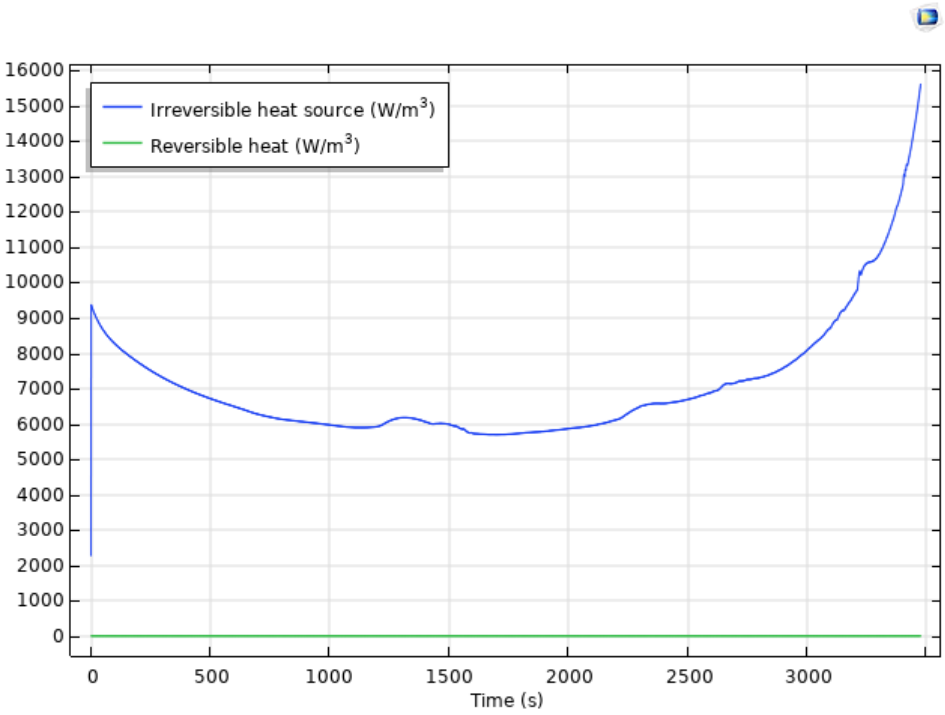

Figure 4.3: Thermal contributions of the structural cell at 1C discharge

It is noted that the heat dissipated from the structural battery cell in the discharge process is mainly composed of the irreversible heat (which is related to the ohmic losses), while the reversible heat (which is related to the entropy change) has been ignored. The result is used to simplify the heat sources in the thermal analysis. Moreover, the irreversible heat has a rising trend as the battery discharges, this is due to the charge transfer resistance increases with the progress of discharging. This corresponds well the resistance study of Onda and the co-workers [26].

Then, different current rates are selected to test the thermal model and do the validation, shown in Figure 4.4.

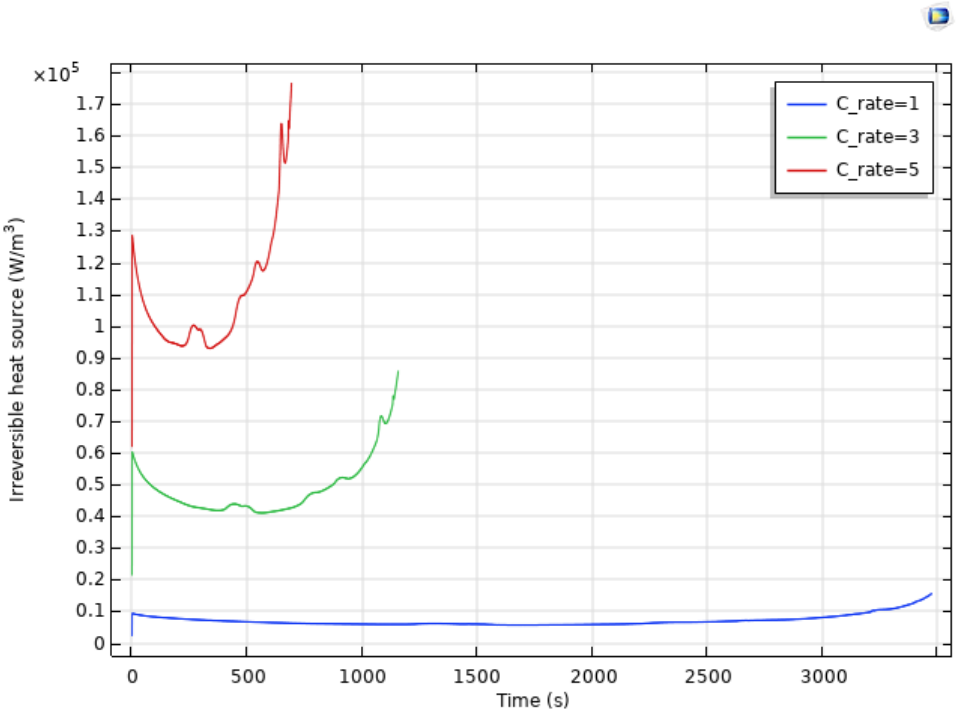

Figure 4.4: Power dissipation at different current rates

At high rates, the power dissipated from the battery model increases dramatically. This result can be explained by (4.2), which is derived by neglecting the reversible term in Eq (2.18).

$$Q_{gen} = Q_{irr} = I^2 R \tag{4.2}$$

It can be easily found that the irreversible heat increases quadratically with the current pulse. When the current pulse is changed to 3C and 5C, the corresponding power dissipation is expected to rise by 9 and 25 times, which can be proved in the figure as well.

4.3.2 Cell temperature

The temperature of the structural battery cell under different current rates is depicted in Figure 4.5, where all temperature figures were captured at boundary 1. As the discharge rate increases, the cell temperature rises significantly in good agreement with the power dissipation result. It is noted that this result is simulated based on the initial convection condition ($h = 0$).

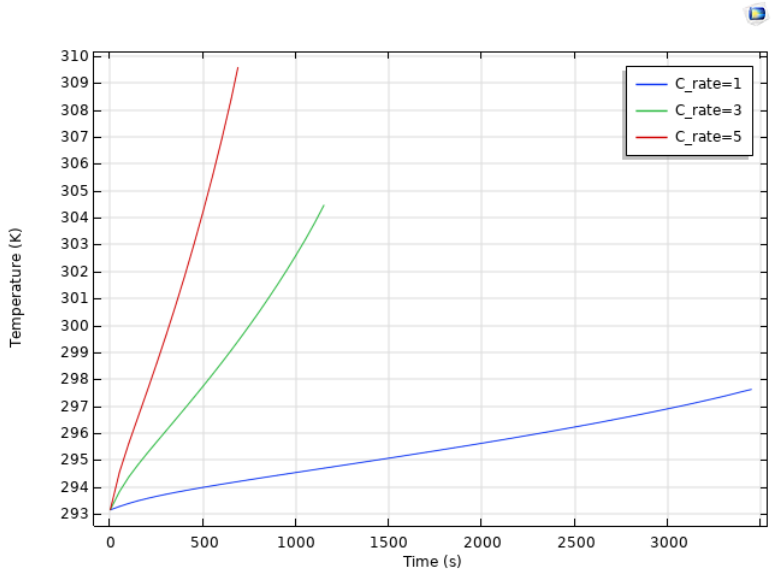

Figure 4.5: Cell temperature under different current rates, captured at boundary 1

4.3.3 The effect of natural convection

Seen from the above, the cell temperature during discharging is highly affected by the current flowing the system. Besides, the heat transfer between the battery surface and its surroundings are also considered in this text in analyzing the thermal behavior of the structural cell. Different heat transfer coefficient h are employed to the 1D model to investigate the thermal impact of natural convection at discharge rate of 1C, 3C, and 5C, seen in Figures below.

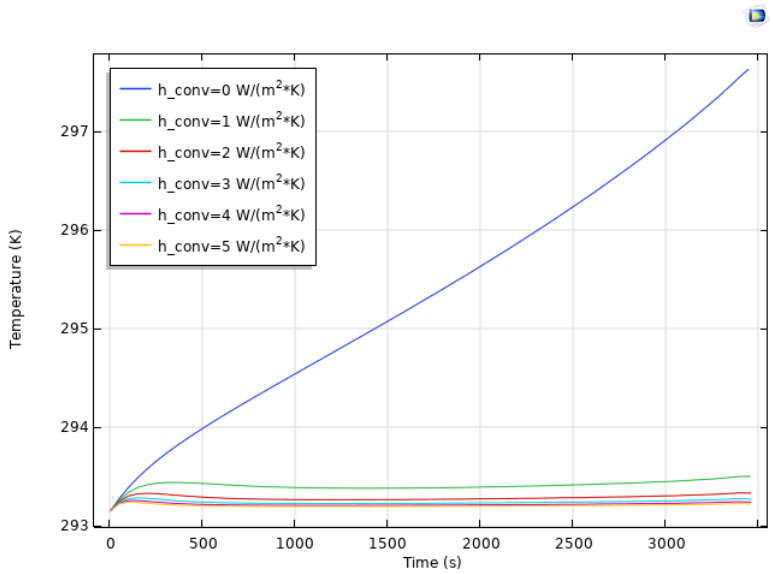

Figure 4.6: Temperature profile at 1C discharge current under different convection

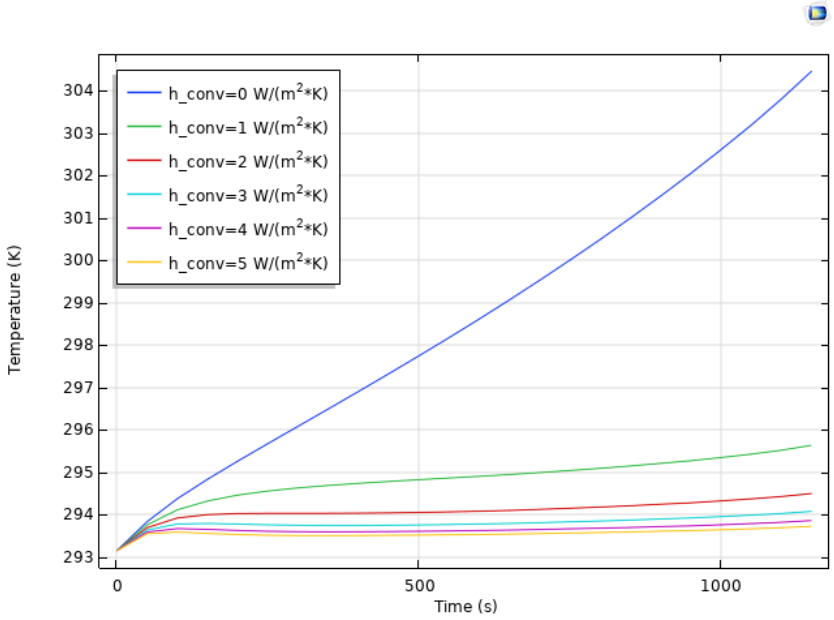

Figure 4.7: Temperature profile at 3C discharge current under different convection

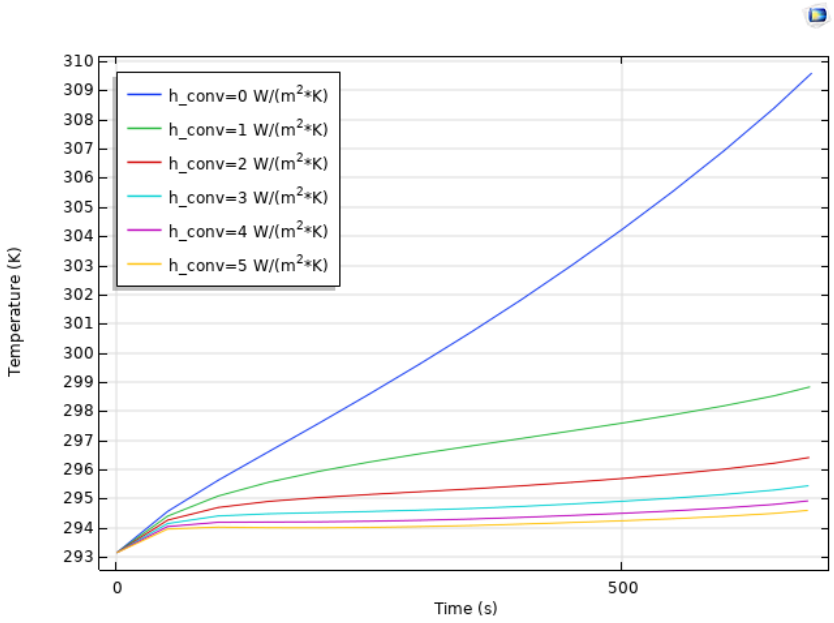

Figure 4.8: Temperature profile at 5C discharge current under different convection

After applying heat convection, the increased rate of cell temperature during discharging has been slowed significantly at all current rates.

For verification, the temperature results in this text have been compared with another MSc thesis (Thermo-mechanical model of structural battery composites) [3]. Specifically, the power dissipation of the P2D electrochemical model is taken as the

input to the 3D thermo-mechanical model, the temperature rise of the battery are shown in Figures 4.9 to 4.12.

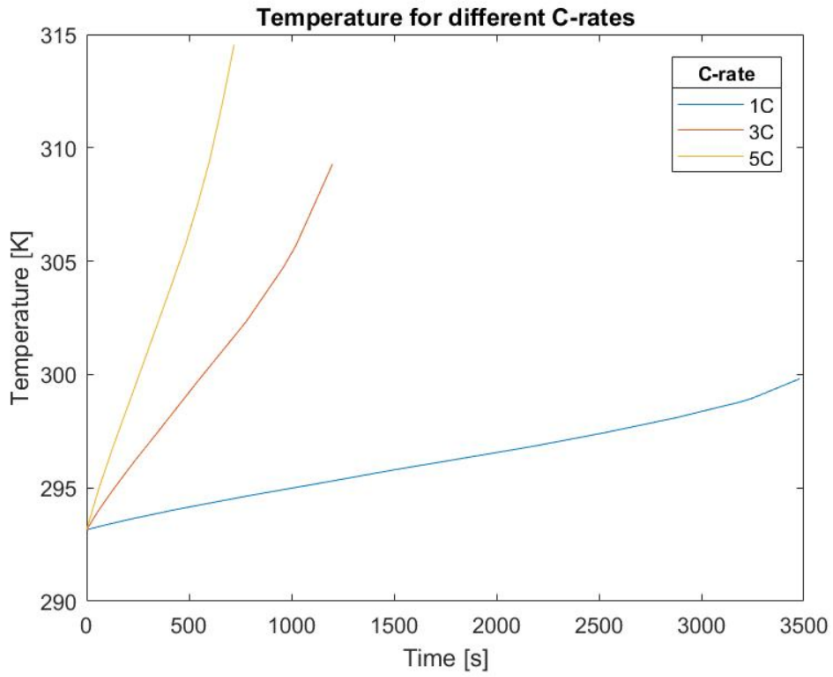

Figure 4.9: Temperature profile at different C rates without natural convection, from [3]

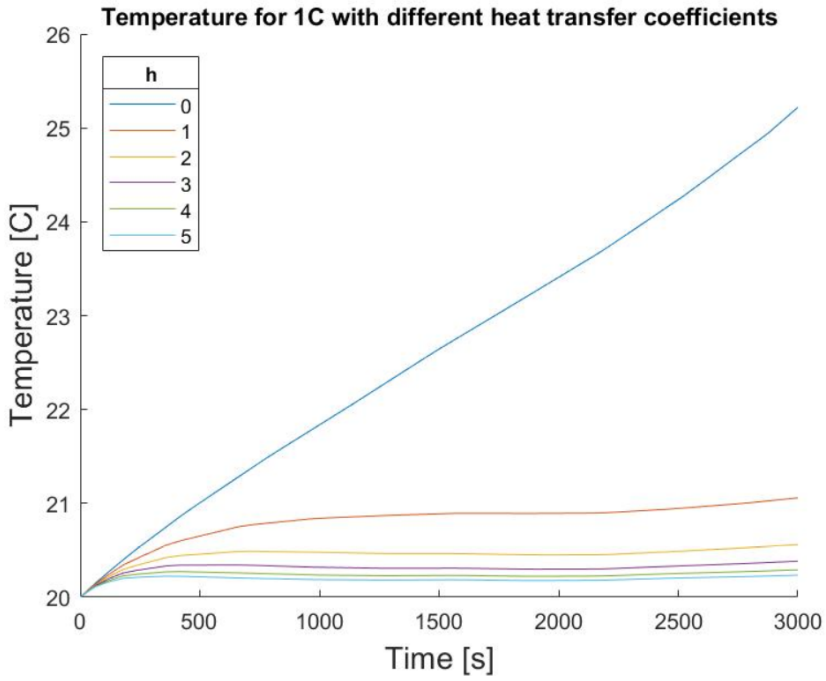

Figure 4.10: 1C temperature profile under convection conditions, from [3]

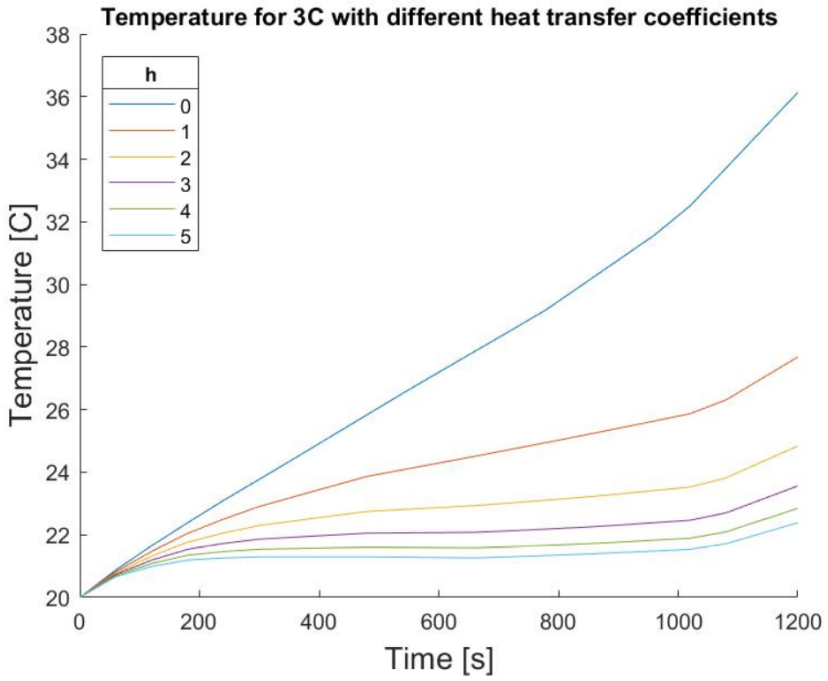

Figure 4.11: 3C temperature profile under convection conditions, from [3]

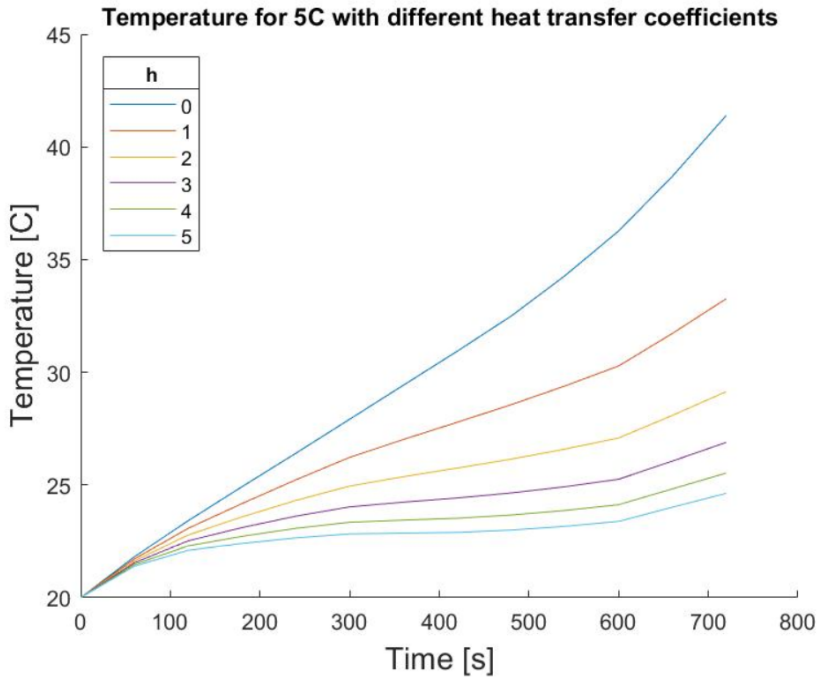

Figure 4.12: 5C temperature profile under convection conditions, from [3]

In addition to the different dimensions of the solid heat transfer simulation, the two models are established based on the same thermal conditions and electrode materials. Figure 4.9 is the temperature curve of the 3D mechanical model during discharging; Figures 4.10 - 4.12 show the heat dissipation impact under different heat transfer

coefficients (h-values). The results agree well to the conclusions obtained before: heat is generated predominantly for high rates and can be dissipated efficiently with natural convection.

5
Conclusion

In order to study the thermal performance of the structural battery cell, a P2D model was established in COMSOL to simulate the thermo-electrical behavior of a structural battery device during the discharge cycle. The FE model is developed based on the energy balance equation of the structural battery, where it is assumed that the heat is generated only by the resistance of the battery components and dissipated to the surrounding environment by convection.

To verify the simulation results, different current rates and convection conditions are used to test the model. For high discharge rates, due to the high contribution of resistance heating, the power generated by the battery increases sharply, and the battery temperature also increases significantly with the discharge time.

This study describes the thermal behavior of structural batteries and compares them with the thermo-mechanical model (established by Svensson [3]). The results from the P2D electrical model have a similar trend to that in the 3D mechanical model, which also enhances the reliability of the modeling results.

Bibliography

[1] Wilhelm Johannisson, Dan Zenkert, and Göran Lindbergh. Model of a structural battery and its potential for system level mass savings. *Multifunctional Materials*, 2(3):035002, 2019.

[2] David Carlstedt and Leif E Asp. Performance analysis framework for structural battery composites in electric vehicles. *Composites Part B: Engineering*, 186:107822, 2020.

[3] Natasha Svensson. Thermo-mechanical modelling of structural battery composites. *Mater thesis in Applied Mechanics, Chalmers University of Technology*, 2020.

[4] Helena Berg. *Batteries for electric vehicles: materials and electrochemistry*. Cambridge university press, 2015.

[5] DJ Johnson. Structure-property relationships in carbon fibres. *Journal of Physics D: Applied Physics*, 20(3):286, 1987.

[6] Giulia Fredi, Steffen Jeschke, Athmane Boulaoued, Joachim Wallenstein, Masoud Rashidi, Fang Liu, Ross Harnden, Dan Zenkert, Johan Hagberg, Göran Lindbergh, et al. Graphitic microstructure and performance of carbon fibre li-ion structural battery electrodes. *Multifunctional Materials*, 1(1):015003, 2018.

[7] Christopher J Orendorff. The role of separators in lithium-ion cell safety. *Electrochemical Society Interface*, 21(2):61, 2012.

[8] Niklas Ihrner, Wilhelm Johannisson, Fabian Sieland, Dan Zenkert, and Mats Johansson. Structural lithium ion battery electrolytes via reaction induced phase-separation. *Journal of Materials Chemistry A*, 5(48):25652–25659, 2017.

[9] Lynn M Schneider, Niklas Ihrner, Dan Zenkert, and Mats Johansson. Bicontinuous electrolytes via thermally initiated polymerization for structural lithium ion batteries. *ACS Applied Energy Materials*, 2(6):4362–4369, 2019.

[10] Thomas B Reddy. *Linden's handbook of batteries*, volume 4. Mcgraw-hill New York, 2011.

[11] David Carlstedt, Johanna Xu, Kenneth Runesson, Fredrik Larsson, and Leif E Asp. Unit cells for multiphysics modelling of structural battery composites. In *Proc. 22nd Int. Conf. on Composite Materials (ICCM22)(Melbourne, Australia,)*, 2019.

[12] DAG Bruggeman. Calculation of different physical constants of heterogen substances i dielectric constants and conductibility of mixtures from isotrop substances. *Annalen der Physik*, 24(8):665–679, 1935.

[13] Marc Doyle. Modeling of galvanostatic charge and discharge of the lithium/polymer/insertion cell. *Journal of The Electrochemical Society*, 140(6):1526, 1993.

[14] Yonghuang Ye, Yixiang Shi, Ningsheng Cai, Jianjun Lee, and Xiangming He. Electro-thermal modeling and experimental validation for lithium ion battery. *Journal of Power Sources*, 199:227–238, 2012.

[15] Karen E Thomas and John Newman. Thermal modeling of porous insertion electrodes. *Journal of the Electrochemical Society*, 150(2):A176–A192, 2003.

[16] Kazuo Onda, Hisashi Kameyama, Takeshi Hanamoto, and Kohei Ito. Experimental study on heat generation behavior of small lithium-ion secondary batteries. *Journal of the Electrochemical Society*, 150(3):A285–A291, 2003.

[17] Y Inui, Y Kobayashi, Y Watanabe, Y Watase, and Y Kitamura. Simulation of temperature distribution in cylindrical and prismatic lithium ion secondary batteries. *Energy Conversion and Management*, 48(7):2103–2109, 2007.

[18] David Carlstedt and Leif E Asp. Thermal and diffusion induced stresses in a structural battery under galvanostatic cycling. *Composites Science and Technology*, 179:69–78, 2019.

[19] Jung-Hoon Song, Seung-Jae You, and Dong Hyup Jeon. Numerical modeling and experimental validation of pouch-type lithium-ion battery. *Journal of Applied Electrochemistry*, 44(9):1013–1023, 2014.

[20] Jane McCann and David Bryson. *Textile-led design for the active ageing population*. Elsevier, 2014.

[21] John Newman and William Tiedemann. Porous-electrode theory with battery applications. *AIChE Journal*, 21(1):25–41, 1975.

[22] John Newman and Karen E Thomas-Alyea. *Electrochemical systems*. John Wiley & Sons, 2012.

[23] Vahur Zadin and Daniel Brandell. Modelling polymer electrolytes for 3d-microbatteries using finite element analysis. *Electrochimica acta*, 57:237–243, 2011.

[24] Maria H Kjell, Tommy Georgios Zavalis, Mårten Behm, and Göran Lindbergh. Electrochemical characterization of lithium intercalation processes of pan-based carbon fibers in a microelectrode system. *Journal of The Electrochemical Society*, 160(9):A1473–A1481, 2013.

[25] Kevin Peuvot, Omid Hosseinaei, Per Tomani, Dan Zenkert, and Göran Lindbergh. Lignin based electrospun carbon fiber anode for sodium ion batteries. *Journal of The Electrochemical Society*, 166(10):A1984–A1990, 2019.

[26] Kazuo Onda, Takamasa Ohshima, Masato Nakayama, Kenichi Fukuda, and Takuto Araki. Thermal behavior of small lithium-ion battery during rapid charge and discharge cycles. *Journal of Power Sources*, 158(1):535 – 542, 2006.